ACSNANO

www.acsnano.org

ARTICLE

On-Demand, Reversible, Ultrasensitive Polymer Membrane Based on Molecular Imprinting Polymer

Nofar Mintz Hemed, Sergio Leal-Ortiz, Eric T. Zhao, and Nicholas A. Melosh*

Cite This: *ACS Nano* 2023, 17, 5632–5643

Read Online

ACCESS | Metrics & More | Article Recommendations | Supporting Information

ABSTRACT: **The development of *in vivo*, longitudinal, real-time monitoring devices is an essential step toward continuous, precision health monitoring. Molecularly imprinted polymers (MIPs) are popular sensor capture agents that are more robust than antibodies and have been used for sensors, drug delivery, affinity separations, assays, and solid-phase extraction. However, MIP sensors are typically limited to one-time use due to their high binding affinity (>10^7 M^{-1}) and slow-release kinetics (<10^{-4} μM/sec). To overcome this challenge, current research has focused on stimuli-responsive MIPs (SR-MIPs), which undergo a conformational change induced by external stimuli to reverse molecular binding, requiring additional chemicals or outside stimuli. Here, we demonstrate fully reversible MIP sensors based on electrostatic repulsion. Once the target analyte is bound within a thin film MIP on an electrode, a small electrical potential successfully releases the bound molecules, enabling repeated, accurate measurements. We demonstrate an electrostatically refreshed dopamine sensor with a 760 pM limit of detection, linear response profile, and accuracy even after 30 sensing−release cycles. These sensors could repeatedly detect <1 nM dopamine released from PC-12 cells *in vitro*, demonstrating they can longitudinally measure low concentrations in complex biological environments without clogging. Our work provides a simple and effective strategy for enhancing the use of MIPs-based biosensors for all charged molecules in continuous, real-time health monitoring and other sensing applications.**

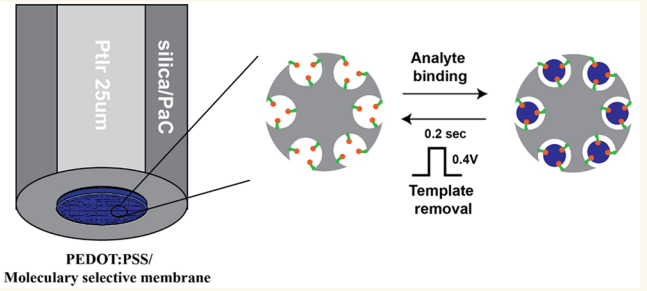

KEYWORDS: *molecular imprinting polymer, dopamine, electrochemical impedance spectroscopy, biosensor, PC-12 cell, reversible, longitudinal real-time health monitoring*

Continuous, real-time health monitoring exhibits significant advantages compared with laboratory diagnostic methods, as it promotes more integrated, informative, timely, and precise diagnoses of human health conditions.[1,2] Developing real-time and longitudinal sensors is a crucial element in achieving continuous health monitoring. The continuous progress of biosensors has enabled the development of chemically specific and highly sensitive biosensors, including optical, electrical, and electrochemical biosensors.[3−6] However, these are generally not applicable to continuous monitoring of health conditions due to sensor clogging and lack of reversibility.

Molecularly imprinted polymers (MIPs), often referred to as synthetic antibodies, are highly selective polymeric materials with molecularly specific binding pockets that have attracted interest in the fields of drug delivery, affinity separations, assays, solid-phase extraction, and biosensors.[7−15] Molecular imprinting is currently one of the most versatile, scalable, and cost-effective approaches to creating tailor-made artificial recognition sites.[14,16] MIP synthesis entails the polymerization of a monomer around the analyte of interest to form selective recognition sites within a synthetic polymer network. The copolymerization takes place in the presence of a functional monomer, a cross-linker, and a target molecule (template).[17] Complementary interactions (either covalent or noncovalent) between the functional monomer and the target molecule create a molecular complex that is then locked into the polymerizing polymer. After polymerization, the template molecule is physically removed from the polymer through washing, cleavage of chemical bonds, or ligand exchange, leaving complementary cavities of the target molecule.[18] These cavities preserve not only

Received: November 21, 2022
Accepted: March 8, 2023
Published: March 13, 2023

https://doi.org/10.1021/acsnano.2c11618
ACS Nano 2023, 17, 5632−5643

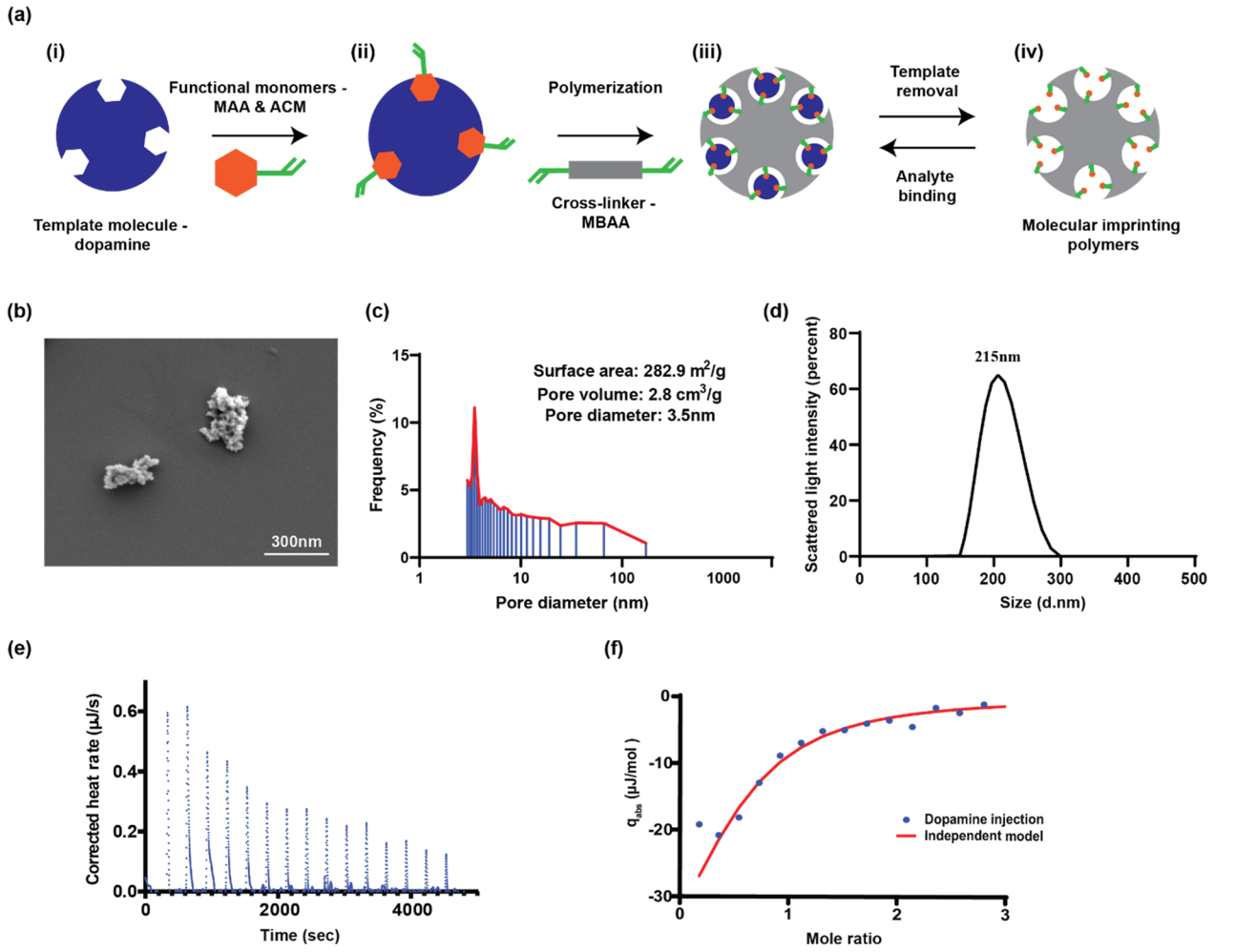

Figure 1. (a) Illustration of the MIPs' preparation, including the following steps: (i) the template molecule, dopamine, (ii) together with the functional monomers (MAA and ACM), (iii) are polymerized in the presence of a cross-linker, (iv) followed by template removal by multiple rinses. (b) SEM image of the MIP particles demonstrates irregularly shaped particles composed of aggregates nanospheres with a rough surface. (c) Pore size distribution for dopamine-MIPs, demonstrating pore size of ∼3.5 nM. (d) MIPs DLS size distribution exhibits an aggregate particle size of 215 ± 12.96 nm. (e) MIPs ITC corrected experimental titration curves, showing the heat generated during gradual injection of the suspension of dopamine into MIPs solution versus time. (f) Observed titration heat versus molar ratio dopamine to MIPs, fit to a single binding site model. The enthalpy of this reaction is exothermic and corresponds to −15.2 kJ·mol^{-1}.

the structure of the target molecule but also the molecular interactions necessary for the recognition of the target. These interactions rely upon weak noncovalent interactions, such as hydrogen bonding, electrostatic attraction, and hydrophobic regions within the templated pocket to form a molecularly selective binding site. Compared with other nonenzymatic biosensors (antibody and aptamers-based biosensors), MIPs benefit from rapid, simple, and low-cost synthesis, providing high selectivity with excellent chemical and thermal stability.[19−22]

Despite the great success of MIPs as a recognition element, some bottlenecks limit their further development for longitudinal sensors, particularly the trade-off between binding affinity and reversibility.[23−28] One of the most important MIP properties for sensor applications is high binding affinity (the strength of interaction between the analyte and the MIP) to the target molecule. High binding affinity is critical for reaching picomolar−nanomolar limits of detection (LOD), which are common analyte concentrations in biological samples, and is often correlated with high specificity and sensitivity.[29] Therefore, MIPs with a very high binding affinity would appear optimal. However, high binding affinity also results in irreversible or very slow analyte release kinetics,[30,31] limiting MIP-based sensors to one-time use applications. For longitudinal or real-time monitoring devices, fast on/off kinetics is equally important as sensitivity and specificity.[32]

In response to this issue, researchers have recently designed stimuli-responsive MIPs (SR-MIPs) to tackle the trade-off between binding affinity and on/off kinetics.[33] In contrast to standard MIP matrixes with a high level of cross-linking, SR-MIPs utilize materials with physicochemical properties that change in response to external stimuli such as temperature, light, magnetic fields, pH, biomolecules, ions, or solvents.[34] These stimuli trigger transitions in the MIPs such as swelling/deswelling, changes in hydrophilicity, cis/trans isomerization, or oxidation/reduction reactions, allowing for the release of the target molecule from the MIPs matrixes. The combination of stimuli-responsive materials and the molecular imprinting technique enabled high selectivity with binding kinetics controlled by simple stimuli response.[34,35] However, these are often difficult to implement, particularly for biomedical devices,

https://doi.org/10.1021/acsnano.2c11618
ACS Nano 2023, 17, 5632−5643

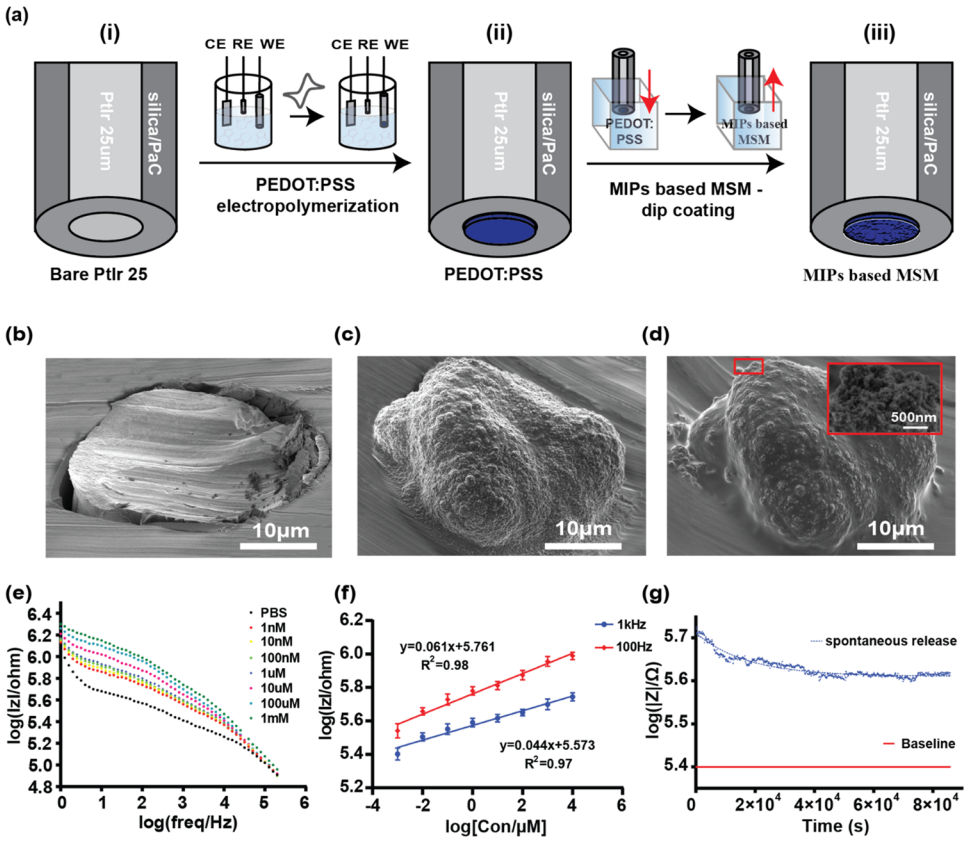

Figure 2. (a) Illustration of the preparation of the microwire MIP-based sensor: (i) silica/PaC insulated PtIr 25 μm microwire with a 25 μm disc exposed on the tip, (ii) functionalized electropolymerized PEDOT:PSS/PtIr microwire on the PtIr tip, and (iii) dip coated MIPs based MSM/PEDOT:PSS/PtIr microwire. (b–d) Corresponding SEM images of the preparation steps of the microwire sensor, bare microwire, PEDOT:PSS functionalized microwire, and MIPs based MSM/PEDOT:PSS functionalized microwire, respectively. Inset of d demonstrates the porous structure with nanopores in size range of a few nanometers. (e) Calibration of impedance amplitude versus frequency over 1 nM–1 mM dopamine concentration (LOD 0.76 nM). (f) Linear fit of log dopamine concentration vs log impedance amplitudes at 100 Hz and 1 kHz. (g) Impedance measurements at 1 kHz of the MIPs-based sensor in 1× PBS at room temperature after detecting 10 μM dopamine, demonstrating limited spontaneous release over 24 h, plateauing at a value of 1 μM dopamine. The decay indicates the sensor's high affinity and slow release rate.

where additional solvents, pH temperature and other chemicals cannot be used.[37]

In the current study, we describe a different mechanism suitable for long-term continuous sensing using traditional highly cross-linked MIPs, including within biological environments. Instead of changing the MIP network itself in response to external stimuli, we tune the interaction between the target molecule and polymer network using electrical potential. As a demonstration, we developed a dopamine-binding MIP with a LOD in the sub-nanomolar range. Our sensor consists of PtIr microwire functionalized with a conductive polymer, and a thin layer consists of MIP particles embedded in a PVC matrix responsible for binding the target of interest. The working principle of the MIP sensor is that the analyte of interest binds in the MIP recognition cavities, impeding ion motion through the MIP to the electrode surface, thus increasing the AC impedance of the entire system. The higher the target molecule concentration, the higher the overall system impedance, until saturation of the membrane is achieved and no further impedance increase is possible.[38-40] After binding dopamine and sensing its concentration, the dopamine is released by applying a positive potential step, which causes to electrostatic repulsion of dopamine out of the polymer matrix.[16]

This approach enables facile modulation of the noncovalent interactions between the MIP and target molecule without changing the MIP's internal properties. We demonstrate repeated binding and releasing by performing 30 sensing cycles. We further validated our system by detecting < nanomolar dopamine release from neuron-like PC-12 cells, demonstrating longitudinal sensing of cellular activity within a biological environment.

The current approach not only simplifies the MIPs synthesis for sensors compared with the SR-MIPs but also maintains all the other MIP's outstanding properties. This is a critical step toward multiuse, small-form factor MIP-based biosensors in continuous, real-time, and health monitoring diagnostics.

RESULTS AND DISCUSSION

MIPs Polymerization and Characterization. Figure 1a illustrates the polymerization process of the MIPs. Briefly, dopamine was combined with functional monomers (methacrylic acid (MAA) and acrylamide (ACM)) to form a molecular complex *via* noncovalent bonds. Under thermal conditions (60°C), the complex was polymerized in the presence of the cross-linker (*N*,*N*′-methylenebis(acrylamide)) and initiator (2,2′-azobis(1-methyl-propionitrile)). The resulting MIP formed a hard white polymer, which was then

https://doi.org/10.1021/acsnano.2c11618
ACS Nano 2023, 17, 5632–5643

powdered using a mortar and pestle and washed three times using the polymerization solvent (methanol/water 4:1 v/v). Dopamine molecules were extracted from the polymer during washing due to the higher solubility of dopamine in the solvent. Nonimprinted polymers (NIPs) were prepared as a control using the same protocol but without dopamine. The properties of the MIP and NIP particles were examined using scanning electron microscopy (SEM), dynamic light scattering (DLS), and isothermal titration calorimetry (ITC).

An SEM image of the resulting MIPs and NIPs particles is shown in Figure 1b and Figure S1a, respectively. The structures of both MIPs and the NIPs particles after grinding were irregularly shaped particles composed of aggregates of nanospheres with the morphology of the individual nanospheres still clearly visible. In comparison between the MIPs and the NIPs morphologies, the MIPs exhibit a slightly rougher surface morphology, possibly due to polymerization in the presence of the dopamine template.[36] However, the larger difference between templated and nontemplated MIPs was in the particle porosity as would be expected if molecular binding pockets had been formed. The specific surface area and pore size of MIP and NIP particles were assessed with Brunauer−Emmett−Teller (BET) adsorption measurements. The specific surface area of MIPs was found to be 282.9 m2/g, compared to only 18.4 m2/g for NIPs, indicating the templated MIP had dramatically higher porosity. Adsorption−desorption isotherms of MIP and NIP polymers exhibit mesoporous (∼3.5 nm) pore structure and exhibit small hysteresis between adsorption and desorption curves resulting from capillary condensation. The pores size distribution was calculated from the experimental isotherms using the Kelvin model of pore filling and the Barrett−Joyner−Halenda (BJH) method (Figure 1c and Figure S1b). These measurements show that the MIP synthesis successfully created highly porous nanoparticles templated from dopamine. DLS was used to characterize the MIP nanoparticle size distribution, shown in Figure 1d. All the particles were dispersed in ethanol by sonication for 30 min and then measured. The MIP nanoparticles are in the range 215 ± 12.96 nm, while the NIP particles were slightly larger at 227 ± 25.45 nm (Figure S1c). The size variation is likely a combination of both the synthesis and the grinding process yet was consistent between batches.

ITC measurements were then conducted to determine the thermodynamic binding affinity of dopamine within the MIPs and the NIPs particles, indicating how strong a binding pocket had been created in each case. Figure 1e shows the heat generated during sequential dopamine injections into a MIP solution versus time. The area of each peak is integrated and plotted versus the molar ratio of the MIP:dopamine (Figure 1f). The quantity of heat produced during dopamine injection is directly proportional to the MIP-dopamine binding affinity. Next, the resulting isotherm was fit with a single uniform binding site model (Figure 1f, solid line) to determine the enthalpy (ΔH) of the MIPs−dopamine interaction, which was calculated to be −15.2 kJ·mol^{-1}. The enthalpy is exothermic and on the higher end of previously reported MIPs enthalpies, representing strong binding properties (comparable or slightly lower to some natural antibodies).[37−39] The enthalpy of the corresponding NIPs was only −0.7 kJ·mol^{-1}, indicating no thermodynamically based binding effect on the NIPs (Figure S1d,e).

Sensor Fabrication and Characterization. A sensor was then constructed using the MIPS particles as the binding agent. The sensor comprised a conductive microwire coated with two functional layers, a conductive polymer, electropolymerized poly(ethylenedioxythiophene):poly(styrenesulfonate) (PEDOT:PSS), and a molecularly selective membrane (MSM) biorecognition based on dopamine MIPs. Figure 2a shows the schematics of the fabrication process. A 25 μM diameter PtIr microwire was first coated with an insulator, Parylene-C (PaC). The end of the wire was then cut, exposing the 25 μM diameter tip, which was then functionalized using electropolymerized PEDOT:PSS to decrease the sensor impedance (Figure 2a). Next, MIP particles were suspended in poly(vinyl chloride) (PVC) solution (Materials and Methods) followed by dip-coating the microwire into the PVC-MIP solution to form a MSM biorecognition MIP layer on top of the PEDOT:PSS layer.

SEM images of the fabrication steps are shown in Figure 2b−d, showing the cut tip of the microwire, PEDOT:PSS/microwire, and MSM MIP/PEDOT:PSS/microwire, respectively. The PEDOT:PSS granular structure has a higher electrode surface area than the flat PtIr microwire, decreasing sensor impedance. After dip coating, the MSM layer formed a thin film (∼100−200 nm, Figure S2a) over the wire and PEDOT functionalized tip area consisting of MIPS particles bound together with a thin layer of PVC. The morphology of the MSM layer for the MIP is shown in the Figure 2d inset. These images show that the MIP-based layer has a porous structure with nanopores, while the MSM layer based on the NIP displays a significantly less porosity structure (Figure S2b,c).

The sensor's electrical properties were then measured to assess the impact of the PEDOT and MSM layers. The device impedance was compared between PaC insulted microwires with a bare PtIr tip and with a PEDOT:PSS functionalized tip using impedance spectroscopy at frequencies ranging from 0.1 to 1 MHz in 1× PBS solution. At 1 kHz, the bare microwires had an impedance modulus of ∼1 MΩ, while the modulus of the PEDOT:PSS polymerized microwires dropped by 2 orders of magnitude to ∼15 kΩ at 1 kHz (Figure S2d). A small impedance variation from sample to sample was observed, caused by synthesis differences in the PEDOT:PSS layer thicknesses. The impedance phase angle changed significantly with PEDOT functionalization, dropping from −65° to −10°, demonstrating that the microwire properties change from capacitive to resistive (Figure S2e), consistent with previous research on PEDOT:PSS coating.[40−43]

The second critical aspect of the sensor, molecular recognition, was tested after dip coating the PEDOT:PSS polymerized microwire in MSM biorecognition MIPs. The sensor impedance with the MSM layer was higher than the PEDOT:PSS microwire device, increasing to ∼150 kΩ at 1 kHz (Figure S2c), with no significant change in the phase (Figure S2d). This impedance increase reflects the increased difficulty of ions moving through the MSM layer in response to an electrical field.

The device's sensing response was examined over a 1 nM−1 mM dopamine concentration range, covering typical physiological ranges and above. A linear correlation between the impedance magnitude and dopamine concentration was observed in a frequency range of 1 Hz−30 kHz (Figure 2e), with a LOD of 760 pM (at 100 Hz, where LOD = 3.3·σ/S, σ is the standard deviation and S is the slope). The impedance values start to converge at higher frequencies, which is consistent with the proposed ion-blocking model. Usually, the impedance in the high-frequency range is characteristic of the electrolyte resistance, while the charge-transfer resistance mostly affects the medium-frequency range. In the low-frequency range, the

https://doi.org/10.1021/acsnano.2c11618
ACS Nano 2023, 17, 5632−5643

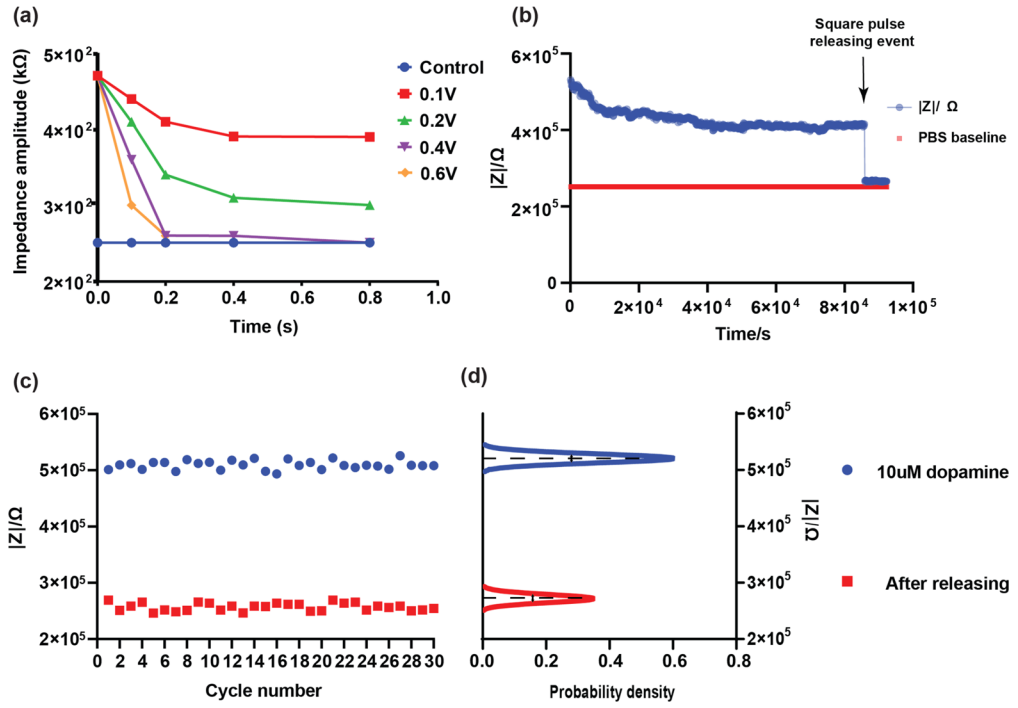

Figure 3. (a) Effect of pulse amplitude (0.1, 0.2, 0.4, and 0.6 V) and duration (0.1, 0.2, 0.4, and 0.8 s) on the releasing event. (b) Impedance measurements at 1 kHz of the MIPs-based sensor in 1× PBS at room temperature after detecting 10 μM dopamine, followed by releasing event at 24 h. (c) Bode amplitude measured at 1 kHz over 30 binding−releasing cycles and its (d) normal distribution of 30 binding−releasing cycles at 1 kHz, with a mean of 275 ± 8 kΩ and fwhm of 19 kΩ for the PBS solutions and a mean of 501 ± 6 kΩ and an fwhm of 15 kΩ for the 10 μM dopamine solution.

impedance is typically sensitive to the diffusion of ionic species in the system. In the presence of dopamine, we observe a linear increase in the sensor's impedance, especially in the mid and low frequencies. The sensitivity of the MSM-PEDOT device was fit from the impedance amplitude vs dopamine concentration at 100 Hz and 1 kHz (Figure 2f), giving sensitivities of 8.7 and 3.9 kΩ/μM, respectively.

Following these results, several negative controls were performed. The first were measurements of the NIP with the same dopamine concentration measured for the MIP sensors. NIP sensors demonstrated little to no sensitivity toward dopamine (Figure S3a,b), showing that the active MIP particles were essential for the sensing process. The second control examined the MIPs in the presence of epinephrine, a common dopamine interferent.[44] Epinephrine did not change the impedance spectrum (Figure S3c,d), indicating low cross-sensitivity against dopamine that could interfere with the sensing. Next, dihydroxyphenylacetic acid (DOPAC), a dopamine metabolite, was examined. DOPAC had a negligible effect on the impedance spectrum in the opposite direction (decrease in the bode amplitude in response to increasing concentration), implying the cavities' specificity toward dopamine (Figure S4e,f).

Lastly, we measured how quickly the dopamine bound in the MIPs sensor would spontaneously release over time, an essential metric for repeated measurements. The sensor was introduced into a solution of 10 μM dopamine for 3 min, and impedance measurements were carried out three times to verify that the impedance was stable. Next, the sensor was rinsed and immersed with a 1× PBS solution to allow dopamine release out of the sensor. Impedance measurements were made sequentially every 1.5 min over 24 h at room temperature (Figure 2g). The impedance decayed gradually over the first 3 h, reaching a plateau with an average value of ∼400 kΩ after that. This corresponds to a concentration of ∼1 μM dopamine still trapped within the sensor. This indicates that, while the device is highly sensitive (LOD 760 pM), it cannot be used repeatedly for concentrations less than several micromolar due to effectively irreversible binding.

Demonstration of Electrostatic Release. Here, we studied whether electrostatic potentials could accelerate analyte release from the MIP sensors to improve their repeated sensing capabilities at low concentrations, without harming device sensitivity. These experiments used PtIR microwire/PEDOT:PSS/MSM devices that had been saturated with 10 μM dopamine for 3 min and then rinsed and immersed in 1× PBS solution. The impedance was measured at this point as the initial value for each device. In addition, a set of sensors that were never exposed to dopamine were taken as the control impedance, which would be the baseline impedance indicating the complete removal of dopamine. A fixed, constant potential was then applied to each device in 1× PBS using a potentiostat for a given period of time; then, the impedance was measured to determine how much dopamine was released.

The release process was studied for different voltage amplitudes and durations. Our parameter ranges were chosen based on two criteria: the dopamine oxidation potential (∼0.6 V) and dopamine surface charge (slightly positive charge by uncharged amine or a charged ammonium species at physiological pH). The applied potentials were thus tested at 0.1, 0.2, 0.4, and 0.6 V, each with a duration of 0.1, 0.2, 0.4, and 0.8 s. These potentials were chosen to probe different possible release mechanisms, as 0.1 and 0.2 V are positive and would electrostatically repel dopamine molecules yet would have slow oxidation rates. Potentials of 0.4 and 0.6 V oxidize dopamine

https://doi.org/10.1021/acsnano.2c11618
ACS Nano 2023, 17, 5632−5643

Table 1. Comparison of Different MIPs-Based Sensors for the Determination of DA

electrode	detection method	linear range (μM)	LOD (nM)	reversible	ref
PPy/carbon nanotubes/MIPs	DPV	5×10^{-5} −5	0.01	no	46
imprinted silica matrix/poly(aniline boronic acid)/Au	DPV	0.05−500	18	no	47
polypyrrole/ZIF-67-MIPs/Nafion/glassy carbon electrode	amperometric/cv	0.08−500	31	no	48
MIP-modified core/shell $CdTe_{0.5}S_{0.5}$/ZnS quantum dots	fluorescence	2.63−26.3	6.6	with washing	49
MIPs/thionine/nanoporous gold	DPV	0.3−100	100	no	50
MIP/nanoporous gold leaf/glassy carbon electrode	DPV	2−180	0.3	no	51
MIPs/PEDOT:PSS/glassy carbon electrode	potentiometric	0.2−10	0.15	with a pH change	52
MIP/functional thia-bilane/pencil graphite electrode	DPV	0.05−250	20	with a pH change/in methylene chloride	53
organic electrochemical transistor	I−V	0.4−10	34	no	54
MIPS/PEDOT:PSS/microwire	EIS	10^{-3} − 10^{4}	0.76	with a small voltage pulse	current work

readily but at exponentially different rates according to the Butler−Volmer equation.[45]

The impedance amplitudes after each applied potential amplitude and duration are shown in Figure 3a and Table S1. Application of the potential dramatically reduced sensor impedance in all cases, indicating that dopamine was being effectively removed from the devices. The change in impedance occurred rapidly, with large changes between 0.1 and 0.4 s, and then plateauing by 0.6 s in all cases. At the smallest, 0.1 V potential amplitude, impedance changes were observed at 0.1 and 0.2 s, reaching a ∼ 25% decrease by 0.4 s relative to the control impedance. Since the impedance values were earlier found to be linear with dopamine concentration (Figure 1f), this means ∼25% of the dopamine molecules were released. Longer pulse durations only slightly enhanced release, showing the release mechanism is fast yet limited in its extent at this potential. Increasing the pulse amplitude to 0.2 V enhanced the dopamine release; however, the signal did not return to the baseline even after a 0.8 s pulse, instead plateauing around 66% release.

However, tests with potentials of 0.4 and 0.6 V resulted in nearly full dopamine release by 0.2 s, with the impedance only slightly above the PBS baseline. Further pulse duration increases to 0.6 and 0.8 s resulted in very small changes (0.03 kΩ), indicating almost all dopamine had been released on the 0.2 s time scale. The 0.6 V amplitude pulse resulted in faster dopamine release kinetics than at 0.4 V; however, after a few sensing/releasing cycles, the MSM membrane failed, indicated by a sharp decay of the impedance amplitude valve to a similar value as the PEDOT:PSS functionalized microwire. Significantly, 0.4 V is also below the breakdown voltage of water, making it more compatible with biological systems.

These tests definitively show that small applied potentials can rapidly remove bound analytes from MIP-based sensors. We were curious, however, how this electrically driven release compared with the spontaneous release. We had already observed that spontaneous release plateaued over 24 h; was it possible that these molecules had become more strongly trapped within the MIP over time and perhaps would also resist electrically driven release? To test this idea, we measured spontaneous dopamine release in PBS solution over 24 h, followed by a 0.4 V pulse (Figure 3b). After 24 h, a decrease of ∼0.1 kΩ was observed, indicating that roughly one-third of the dopamine was spontaneously released during this period. Next, we applied a potential step with an amplitude of 0.4 V and duration of 0.2 s, followed by a measurement of the sensor's impedance. An immediate drop in the impedance to the baseline value was observed after the potential step (Figure 3b) to within 4% of the PBS control, indicating almost all dopamine was released. Thus, even after extended periods, the molecules are still quickly removed by modest applied voltages and are tremendously more effective than washing.

A key metric for the electrically driven analyte release is whether the release process damages or changes the sensors' properties, particularly the impedance value for a given analyte concentration. We tested this by repeating the binding−releasing cycles 30 times and measuring the impedance at 10 μM dopamine and after each release cycle (Figure 3c). Each cycle consisted of introducing the sensor into a 10 μM dopamine solution for 3 min and measuring impedance at 1 kHz, then placing the device into 1× PBS and applying 0.4 V for 0.2 s and repeating the impedance measurement. The impedance amplitude consistently cycled between the value for 10 μM dopamine and the control PBS baseline, indicating that dopamine is fully released from the membrane every cycle, and the voltage pulses do not appear to degrade the MSM layer or sensor operation. The impedance values during cycling were highly uniform, with normal distribution fits of 501 ± 6 kΩ for the dopamine solution and 275 ± 8 kΩ after electrically driven release (Figure 3d). These results confirmed that the sensor's sensitivity remained stable over repeated binding/releasing steps, and the applied potential step did not affect the MSM binding properties.

The microwire MIPs-based sensor analytical performance, including the reversibility property, was compared to previously reported dopamine MIPs-based sensors, as shown in Table 1. This comparison demonstrates that the microwire MIPs-based sensor exhibits good sensitivity and a wide linear range in addition to its longitudinal sensing capability.

Understanding the Release Mechanism. In MIPs, the recognition of the target molecule is based on two principles, the molecule's shape and molecular interactions (e.g., the creation of hydrogen bonds). There are a few ways to increase the MIP's release kinetics. One option is to design MIPs with poor molecular interaction strength, which results in a high dissociation rate (K_D); however, the sensitivity of these sensors is relatively low with a poor LOD. A different option is to apply external stimuli to break the molecular interactions, enabling the release and diffusion of the target molecule out of the matrix. In SR-MIP, a structural change occurs due to molecular binding/reaction of added chemical agents, temperature change, and other external factors that alter the MIP. The current work shows that a mild electrical potential can cause a high percentage

https://doi.org/10.1021/acsnano.2c11618
ACS Nano 2023, 17, 5632−5643

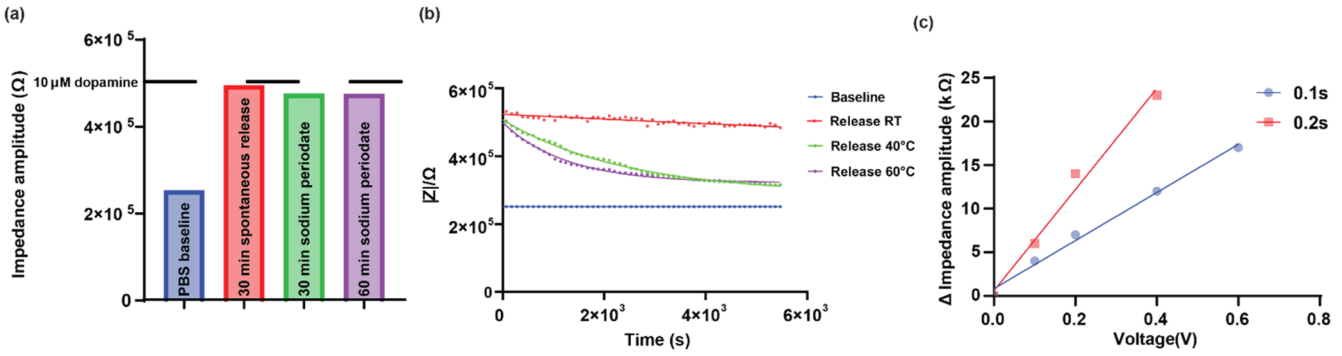

Figure 4. (a) Difference in impedance amplitude between spontaneous release and release enhanced by chemical oxidation using sodium periodate. The immersion in sodium periodate promotes dopamine release; however the signal is not returning to its original baseline (PBS). (b) Impedance amplitude of dopamine release is enhanced by different temperatures (40 and 60 °C). Yet, a full dopamine depletion is not observed as the signal remained above the PBS baseline. Results were fitted to an exponential decay equation model, and the rate constant of the process was extracted and found to be 3.34×10^{-4} and 7.96×10^{-4} s^{-1}, respectively, with temperature. (c) Linear correlation between the pulse amplitude and the release event implies that the primary mechanism is electrostatic repulsion.

of bound molecules to release. We postulate three main mechanisms through which this may occur: oxidation of the dopamine molecules, local Joule heating, or electrostatic repulsion.

First, we investigated whether electrochemical oxidation was the mechanism. Oxidation would alter the molecular dipole moments, weakening the binding strength within the pocket and allowing diffusive release. The complete removal of the analyte near dopamine's oxidation potential (at both 0.4 and 0.6 V) also suggests this could be a possible mechanism. To test this idea independently of the applied voltage, we directly oxidized dopamine within the MIP with a strong chemical oxidizer. After immersing the sensor into 10 μM dopamine solution, rinsing in PBS solution, and measuring the impedance sequentially 3 times (~3 min, showing the signal is stable), the sensor was washed and dipped in 1 mM sodium periodate solution (pH 7.2 at room temperature) for 30/60 min. Sodium periodate is a small, strong oxidizing agent known to oxidize dopamine readily.[55] Following immersion, the sensor was rinsed and the impedance was measured in a clean 1× PBS solution. The change in the impedance amplitude at 100 Hz is shown in Figure 4a. Although the periodate solution slightly enhanced dopamine removal, the impedance decreased by only ~11% compared with a spontaneous release, which decreased by ~2.5% in 30 min and much less than the total release with electrical potential. While we cannot rule out some contribution of electrochemical oxidation, its maximum effect appears to be quite limited.

Next, we examine if it was possible some local heating occurred near the tip, heating the MIP and driving thermal diffusion. This seems unlikely given extremely small currents flow during the release process, yet we wanted to eliminate it as a possibility. Higher temperatures increase the kinetic energy of the molecules, making it easier to overcome the barrier associated with the MIP−dopamine interactions. We repeated the release experiment at two elevated temperatures: 40 and 60 °C. For both experiments, the sensor was first dipped into a 10 μM dopamine solution and rinsed and the impedance was measured in 1× PBS sequentially 3 times (~3 min, showing the signal is stable at room temperature). Next, the sensor was immersed in a clean 1× PBS at 40 and 60 °C and the impedance was measured over 90 min. As expected, the higher the temperature, the faster the release (Figure 4b), and both elevated temperatures gave much faster release than at room temperature, plateauing near 70% release.

However, for thermal diffusion to be the mechanism during the applied voltage experiments it would have had to release over a period of 0.2 s. Based on an Arrhenius activation model, we can calculate the activation energy for dopamine release from the rate constants fit from the thermal release data, $k = 3.34 \times 10^{-4}$ s^{-1} ($R^2 = 0.928$) for 40 °C, and $k = 7.96 \times 10^{-4}$ s^{-1} ($R^2 = 0.987$) for 60 °C. Using the Arrhenius equation, we can calculate the rate constant of the reaction at room temperature $k = 1.31 \times 10^{-4}$ s^{-1} and the energy of the unbinding reaction $E_a \sim 37$ kJ/mol, with a pre-exponential factor of 550 s^{-1}. Interestingly, comparing this to the thermodynamic binding enthalpy calculated from ITC (15.2 kJ/mol) gives an activation energy of ~22 kJ/mol for the reaction, larger than the thermodynamic change itself. This likely reflects the difficulty for molecular release from the small, tailored binding pockets, suggesting MIPs are effective both for their (rather modest) thermodynamic interactions as well as a steric hindrance for molecules to escape. In comparison to the voltage experiments where 95% of the dopamine was released in 0.2 s, to release the same amount of dopamine simply by thermal diffusion will require a temperature of 983°C at the electrode's tip, which is ruled out by the lack of any bubble formation at the tip.

With the other two mechanisms eliminated, we finally turned to electrostatically-driven release. We examined different pulse duration and amplitudes and their effect on the amount of dopamine released, which is reflected as a change in the impedance amplitude. To do that, we further analyzed the results from Figure 3a. Figure 4c plots the effect of the different pulse duration and amplitudes on the releasing event ($\Delta\Omega$). The amount of release is linearly proportional to the applied voltage. This is what we would expect for electrostatically driven phenomena, as the potential away from the electrode scales linearly with applied potential as given by the linearized Poisson−Boltzmann equation, $\Psi(x) = \Psi_0 e^{-x/\lambda_D}$, where Ψ is the electric potential, Ψ_0 is the surface potential, and λ_D is Debye length. If the mechanism was electrochemical oxidation, we would expect an exponential behavior as given by the Butler−Volmer equation, as we are close to dopamine's redox potential of +0.6 V. This demonstrates that electrostatic repulsion of dopamine is the major release mechanism.

The mechanism of dopamine release was studied under different conditions, including a strong chemical oxidizer, different temperatures, and different pulse lengths. Although

https://doi.org/10.1021/acsnano.2c11618
ACS Nano 2023, 17, 5632−5643

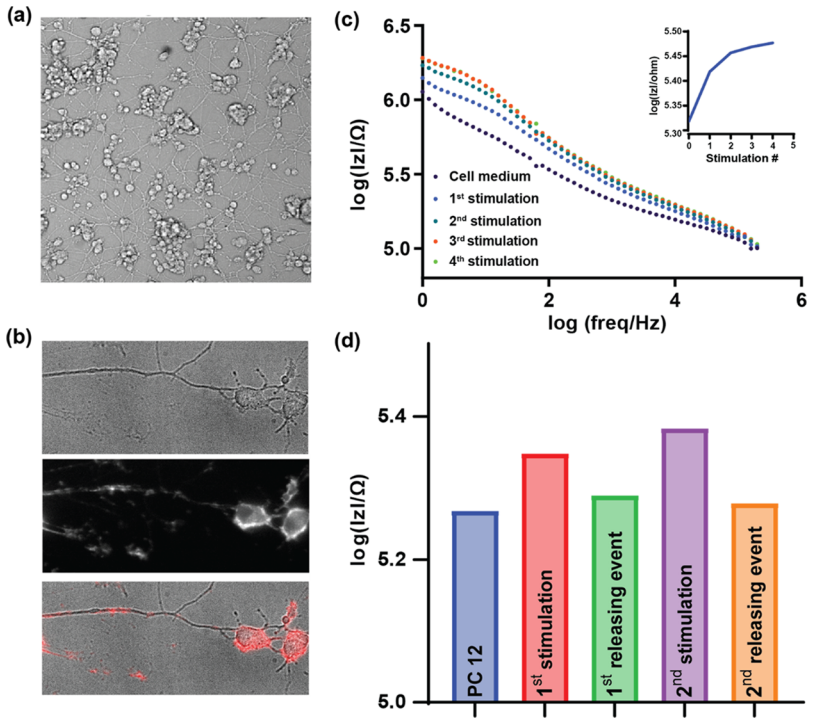

Figure 5. (a) PC-12 cells, 6 days *in vitro* showing the cells' morphology and differentiation. (b) FM dye cycling of PC-12 cells after stimulation, from top to bottom, differential interference contrast microscopy image, FM 4-64 image, and a merged image, demonstrating exocytosis events. Inset is impedance response to (c) sensor's Bode amplitude responds to five subsequent stimulations in 5 min time intervals. The first three stimulations increased impedance amplitude, whereas the 4th stimulation did not result in an additional increase due to the depletion of the dopamine pool. (d) Demonstration of repeated sensing/release events using electrical stimulated PC-12 cell. PC-12 cells were first stimulated to result in a release of dopamine, which was detected by the sensor. Fully dopamine depletion of the sensor was done by applying a square pulse.

different temperatures had enhanced dopamine release, it is unlikely to be the main mechanism as it will require a temperature of 983 °C next to the tip of the electrode. Next, we showed that direct oxidation of dopamine by a strong chemical oxidizer resulted in a small change in the impedance amplitude. Electrochemical oxidation was also ruled out based on the linear correlation between the applied voltage and the change in the impedance amplitude. Therefore, we were able to conclude that the primary release mechanism is electrostatic repulsion, making it suitable for all charged molecules.

Demonstration of Repeated Molecular Detection of Biological Dopamine Using PC-12 Cells. Next, we tested if the dopamine sensor could operate within a biological environment without clogging and be sufficiently sensitive to measure biologically relevant concentrations (picomolar—nanomolar). Microwire sensors were introduced into Petri dishes with a monolayer of dopaminergic PC-12 cells in media (Figure 5a). PC-12 cells have been widely used for neural differentiation and to examine exocytotic release events due to the neurogenic nature acquired after differentiation, such as high level of a secreted neurotransmitter, and expression of ion and neurotransmitter receptors, making them an ideal model to demonstrate longitudinal sensing *in vitro* and *in vivo*. Most usefully for this experiment, PC-12 cells can be electrically stimulated to release dopamine, providing a clear before/after stimulation response. FM dye cycling was performed to confirm the PC-12 cells' synaptic vesicle (SV) activity in response to electrical stimulation. The FM dye is internalized during the SV endocytosis and later released with SV exocytosis, indicating the release of dopamine from the PC-12 cells.[56] A raw FM4-64 dye image (Figure 5b) demonstrates vesicles of a PC-12 synapse stained by FM4-64 dye in the cell body and its neurites, demonstrating exocytotic release in response to electrical stimuli of the PC-12 cell culture, confirming the expiration of dopamine by the PC-12 cells.

Next, the dopamine exocytosis initiated by stimulation of the PC-12 cells was sensed with a MIP sensor immersed inside the cell culture medium. To induce dopamine exocytosis, PC-12 cells (cultured 6 days *in vitro*) were electrically stimulated using two mesh Pt electrodes (50 mm^2) in the culture media with a square wave excitation of 10 Hz, 1 ms long, 30 mA, and 90 s total stimulation. Using electrical stimulation, we were able to demonstrate the sensitivity of the microwire sensor to the increased dopamine concentration, resulted from the stimulated PC-12 cells. Figure 5c shows the sensor response to four sequential stimulations in 5 min intervals. The first stimulation increased sensor impedance at 1 kHz from ∼200 to ∼270 kΩ corresponding with ∼860 pM dopamine. The second and the third stimulations resulted in a further small rise in the signal to ∼281 and ∼295 kΩ, corresponding to ∼1.0 and ∼3 nM dopamine concentration. However, the last stimulation did not cause any appreciable change in sensor impedance. PC-12 cells have two distinct pools of vesicles, the release-ready granule pool and the reserve pool comprising the majority of granules. The lack of change in the impedance after repeated stimulation indicates depletion of the pool of PC-12 releasable vesicles. To confirm this, an additional series of cell stimulation was performed in the same culture after 1 additional day in growth media to renew dopamine production. Figure S4 shows that stimulation of the PC-12 cells further increased the sensor

https://doi.org/10.1021/acsnano.2c11618
ACS Nano 2023, 17, 5632−5643

impedance, indicating the plateau was due to dopamine depletion. These results confirm that the MIPs-based sensor is capable of measuring a biologically relevant concentration (picomolar−nanomolar) resulting from a single exocytosis event in a complex biological media.

As a control measurement, we repeated the simulation experiments with PC-12 cells that were cultured for 15 days, where it is known that PC-12 cells are not induced ny dopamine exocytosis.[57,58] In this case, the PC-12 cells were electrically stimulated using two mesh Pt electrodes (50 mm^2) in the culture media with a square wave excitation of 10 Hz, 1 ms long, 30 mA, and 90 s total stimulation. Figure S5 shows the PC-12 cells' response to the electrical stimulation. However, in this case, the stimulation did not cause any appreciable change in sensor impedance. These results reinforce the sensor's selectivity toward dopamine.

For long-term and continuous use, the sensor must maintain its reliable functionality in a complex *in vivo* environments over time. Therefore, in the next step, we examined the sensor functionality to repeatedly sense dopamine release from PC-12 cells in a biological environment, as biofouling is well-known to cause sensor clogging and degradation. Initially, the sensor was dipped into the cell media and impedance measurement was performed to set the baseline of the experiment. Next, PC-12 cells were stimulated using a square wave excitation of 10 Hz, 1 ms long, 30 mA, and 90 s total stimulation, followed by impedance measurement of the sensor. After the sensing, a release potential step of 0.4 V for 0.2 s was applied to the sensor to release the bound dopamine within the MIP. We performed this stimulation-binding cycle two times in 5 min intervals and measured the impedance spectrum after every step. Dopamine was accurately detected after electrical stimulation of the PC-12 cells. After the 0.4 V cleansing potential, the impedance decreased and returned to its baseline (Figure 5d), indicating that dopamine could be released and the sensor refreshed for the next sensing cycle. These results show that the MIP sensors are capable of detecting biologically relevant dopamine concentrations and can be reused in a biological environment.

CONCLUSION

In summary, we demonstrated a MIP-based sensor that could reversibly detect and release dopamine using a small potential step. This technique does not require complicated MIP fabrication nor the use of complex external components for stimulation (e.g., temperature, light, magnet, pH, biomolecule, ion, or solvent stimulation). Moreover, we found that the release mechanism is controlled by electrostatic repulsion, making it suitable for any charged molecules not just electrochemically active ones. The sensing performance and reversibility were confirmed in solution and in a biological environment using PC-12 cells at the relevant physiological concentrations.

This study provides a simple and easy strategy for improving the MIPs sensor technology by enabling reversibility and repeated sampling while maintaining high sensitivity. This development is important for long monitoring in biological environments and potentially expand the use of MIP devices for real-time monitoring and health care. Further study will be dedicated to *in vivo* monitoring, developing different MIPs for creating sensor arrays, and eventually integrating it with wireless electronics and demonstrating performance after long-term implantation.

MATERIALS AND METHODS

Materials. Dopamine hydrochloride, norepinephrine, *N*,*N*′-methylenebis(acrylamide) (MBAA), methacrylic acid (MAA), acrylamide (ACM), 2,2′-azobis(1-methyl-propionitrile) (AIBN), bis(2-ethylhexyl) adipate, tetrahydrofuran (THF), acetonitrile, 3,4-ethylenedioxythiophene (EDOT), poly(sodium 4-styrenesulfonate) (Mw 70,000), lithium perchlorate, potassium tetrakis(4-chlorophenyl) borate, sodium periodate, and b-NGF of human origin were purchased from MilliporeSigma company (Milwaukee, WI). Methanol, acetic acid, and 1× PBS solution were purchased from Fisher BioReagents. Working standard solutions were prepared fresh daily. All solvents were of either analytical or HPLC grade.

Preparation and Imaging of the Dopamine Molecular Imprinting Polymer. The dopamine−MIP was synthesized by *in situ* polymerizations of the dopamine template, MAA, ACM, and MBAA at a 1:2:2:10 molar ratio. The polymers were synthesized as reported earlier using a method outlined by Suedee et al.[59] using thermal polymerization with AIBN as an initiator. First, the monomeric components, MAA and ACM (both 0.3 M), and the cross-linking monomer, MBAA (1.5M) were dissolved in a methanol/water mixture (25 mL, 4:1, v/v) along with the initiator, AIBN (0.284 gr), and dopamine (0.15M). Subsequently, the mixture was purged with a stream of nitrogen gas for 30 min to remove the radical scavenger oxygen. Copolymerization was performed at 60 °C for 18 h on a hot plate. The resulting polymers were crushed, ground, and sieved through a 100 mesh sieve having an open width of 100 μm. The polymer particles were washed 3 times with 10% v/v acetic acid in methanol (500 mL) and 3 times with portions of methanol (500 mL). The complete removal of the dopamine molecule from the polymer was confirmed by the lack of dopamine in the methanol rinses of the polymer, which was verified using fluorescence spectroscopy. The polymer particles were then dried under a vacuum and stored in airtight containers at room temperature until needed. A control NIP was prepared in the same way as the dopamine−MIP, except that template molecules were not included.

MIPs and NIPs particles were visualized *via* SEM (FEI Wuanta FEG 250). First, the particles were diluted in ethanol and then dispersed on the SEM stage and dried under a vacuum oven. Prior imaging samples were sputter-coated with a 5 nm Au/Pd (60:40 ratio) layer to ensure electrical conductivity.

BET Measurement. The specific surface area of the MIPs and MIPs was evaluated by nitrogen physiosorption using a BET Quantachrome Autosorb iQ3 instrument. The samples were degassed under a vacuum at 80 °C for 6 h before analysis. The pore size was determined using the desorption isotherms in a relative pressure window of 0.35 to 0.99 and following the BJH approach.

Isothermal Titration Calorimetry. All the ITC experiments were performed using the Nano ITC instrument. All the reagents were dissolved in DI water and filtered through a 1 μm PVDF filter with a Luer lock syringe. Prior to the titration, the solutions were degassed. For most experiments, a total of 50 μL of dopamine (50 mM) was injected into the reaction cell containing 250 μL of MIP solution (240 μg/mL) at 25 °C. The titrant was injected at 120 s intervals to ensure that the titration peak returned to the baseline before the next injection. For a control experiment, 50 μL of dopamine (50 mM) was titrated into a 2 mg/mL NIP solution. The dopamine concentration was determined based on the following equation $c = nP_t/K_d$", where P_t is the analyte concentration in the measurement cell, n is the number of binding sites per MIP, and K_d is the affinity constant, which must fall between 20 and 100 to yield an accurate estimate of K_d, ΔH, ΔS, and n.[60]

A background titration, consisting of DI water into MIPs solution, was recorded each time to account for the heat of dilution and background signal (Figure S1f).

Preparation of the Sensing Electrodes. *Microwire Insulation.* To prepare the sensing electrodes, a 25 μm PtIr microwire was purchased from Goodfellow Inc. Using a custom spooling rig, microwires were wrapped from their spool onto a custom rack wherein each wire was insulated by the following; first, silica deposition was done at 300 °C in a low-pressure chemical vapor deposition furnace

https://doi.org/10.1021/acsnano.2c11618
ACS Nano 2023, 17, 5632−5643

(Stanford Nanofabrication Facility). A custom rack allowed for >1 km of microwire to be coated at the same time. PaC was deposited using chemical vapor deposition (SCS Labcoater 2) to the desired thickness using the same rack. Subsequently, wires were cut, and each microwire was individually hand soldered.

Electrochemical Polymerization. PEDOT:PSS electropolymerization was performed to increase the sensing electrodes' active area and lower the electrode−electrolyte impedance. The process of electrochemical polymerization was performed by means of SP-200 potentiostat (biologic) in a three-electrode setup, comprising a Pt wire as the counter electrode (CE), Ag/AgCl as a reference electrode (RE), and the insulated PtIr microwire as the working electrode. PEDOT:PSS was deposited from 10 mM EDOT and 0.1 mM NaPSS containing 0.1 M $LiClO_4$ as the supporting electrolyte in a solvent mixture of acetonitrile/DI water (1:1 v/v).[61] Cyclic voltammetric (CV) curves were collected at 50 mV s^{-1} for 10 CV cycles within the potential range of −0.8−1.8 V based on the electrochemical windows.[62] The protocol involved changing the oxidation potential of the polymerization process in order to form a polymer with superior electrochemical characteristics in terms of high charge storage capacity and low impedance modulus around 1 kHz.[63]

Molecularly Selective Membrane Coating. The molecularly selective membrane was coated on top of the electropolymerized PEDOT:PSS by dip coating a tetrahydrofuran (2 mL) mixture containing the dopamine MIPs, a high molecular weight PVC (51.0 mg), the bis(2-ethylhexyl) plasticizing solvent mediator (120.0 μL), and the anion excluder potassium tetrakis(4-chloropheny1) borate (15.0 mg).[64] Dip coating was performed using NIMA Technology Micro-Processor Interface IU4, at three different speeds (10, 50, and 100 cm^2/min), in order to optimize the molecularly selective membrane thickness. The dip-coated wires were dried overnight in airtight containers at ambient temperature.

Sensing Electrodes Characterization. *Scanning Electron Microscopy.* The microwire-based sensor was visualized *via* SEM (FEI Wuanta FEG 250) after every fabrication step and after the *in vitro* measurements. Prior imaging samples were sputter-coated with a 5 nm Au/Pd (60:40 ratio) layer to ensure electrical conductivity.

Electrochemical Impedance Spectroscopy. Electrochemical measurements were performed after each of the functionalization steps and later after every sensing and releasing step. The measurements were performed in a conventional three-electrode-electrochemical cell composed of PtIr microwire/our sensor as the working electrode, platinum wire as a counter electrode, and an Ag/AgCl reference electrode. Impedance characteristics were performed in the frequency range 1 Hz−200 kHz (10 points per decade), under open circuit potential with 10 mV modulation voltage, using potentiostat/galvanostat (SP-200, BioLogic science instruments Ltd.). For the electrode characterization, the electrolyte used was 200 μL of PBS solution, at pH = 7.45 at room temperature. For the sensor calibration, the electrolyte was a dopamine solution in a concentration range of 1 nm −1 mM. For the PC-12 cells experiments, the solution was RPMI-1640 medium.

Dopamine Release. The release potential step was performed using a conventional three-electrode-electrochemical cell composed of PtIr microwire/our sensor as the working electrode, platinum wire as a counter electrode, and an Ag/AgCl reference electrode. A small potential step with an amplitude of 0.4 V and duration of 0.2 s.

PC-12 Cell Culture. PC-12 cells were generous to obtain from ATCC American Type culture collection catalog number CRL-1721. The cells were grown in 25 cm^2, 75 cm^2, tissue culture flasks, and 6-well plates 30 mm in diameter with RPMI-1640 medium. To make the complete growth medium was added the following components to the base medium: heat-inactivated horse serum to a final concentration of 10%, fetal bovine serum to a final concentration of 5%, and penicillin−streptomycin 1× final concentration.[57,65]

Cultures were maintained according to standard protocols at 37 °C with 5% CO_2/95% air in a humidified incubator. Cells at passages 4−6 (passage number after receipt) were thawed once every 2 weeks and were grown for 7 days with one passage in between for maintenance. On the sixth day, the cells were passaged and divided for maintenance in culture and for the experiment in different media depending on the experiment. To minimize variability, all the experiments were performed with cells in passages between 6 and 10.[57]

PC-12 Cell Plating and Differentiation. Cell culture plates were coatings with PDL or Matrigel for 24 h before culture. PC-12 cells were differentiated using b-NGF of human origin (Sigma-Aldrich, cat. no. SRP3015) at a concentration of 100 ng/mL.[66] The culture medium was changed 24 h after plating for the first time and changed every 48−72 h after. The cells were cultured for the experiment on days 4, 6, 8, and 10 of incubation with 100 ng/mL rat NGF. In these assays, cells were cultured in two different densities, 50 000 and 100 000 cells. Cell differentiation using NGF results in a dense network of neurites.

Dopamine Detection Measurements with PC-12 Cells. In order to induce endocytosis from PC-12 cells, the cells were stimulated at a frequency of 10 Hz, 1 ms, and 30 mA for 5 min. Impedance measurements were performed after every electrical stimulation as detailed before.

PC-12 FM Dye Cycling loading. Functional presynaptic boutons from PC-12 culture were labeled with FM4-64 dye (Invitrogen) by incubation in regular media containing ∼1 μg/mL FM dye for 60 s followed by electrical stimulation at the frequency of 40 Hz 30 mA, 0.1s for 5 min, followed by three washes of 1 min each before to perform an image. The PC-12 cells were then imaged with an inverted fluorescence microscope (Zeiss Axiovert 200M).

ASSOCIATED CONTENT

Supporting Information

The Supporting Information is available free of charge at https://pubs.acs.org/doi/10.1021/acsnano.2c11618.

> Figures of NIPs characterization including SEM images, DLS, BET, size distribution, and ITC dynamics, comparison between MSM-MIPs and MSM NIPs, characterization of the different stages of the microwire sensor preparation, control measurement using the NIP's MSM, epinephrine as a structural analogue, and DOPAC, as dopamine metabolite, sensor responding to five PC-12 cells stimulations, and control measurement with cells that have been cultured 15 days *in vitro* and table of impedance change as a result to different releasing process (PDF)

AUTHOR INFORMATION

Corresponding Author

Nicholas A. Melosh − *Department of Materials Science and Engineering, Stanford University, Stanford, California 94305, United States;* orcid.org/0000-0002-2601-1379; Email: nmelosh@stanford.edu

Authors

Nofar Mintz Hemed − *Department of Materials Science and Engineering, Stanford University, Stanford, California 94305, United States;* orcid.org/0000-0002-8312-5989

Sergio Leal-Ortiz − *Department of Psychiatry and Behavioral Sciences, Stanford University, Stanford, California 94304, United States*

Eric T. Zhao − *Department of Chemical Engineering, Stanford University, Stanford, California 94305, United States*

Complete contact information is available at: https://pubs.acs.org/10.1021/acsnano.2c11618

Notes

The authors declare no competing financial interest.

https://doi.org/10.1021/acsnano.2c11618
ACS Nano 2023, 17, 5632−5643

ACKNOWLEDGMENTS

Research at Stanford was supported by the Wu Tsai Institute Big Ideas program. N.M.H. was supported by the Schmidt Futures program, the Israeli Council for Higher Education, and Ben-Gurion University Postdoctoral Award Program for Advancing Women in Science. Part of this work was performed at the Stanford Nanofabrication Facility (SNF), supported by the National Science Foundation under award ECCS-2026822

REFERENCES

(1) Vashist, S. K. Point-of-Care Diagnostics: Recent Advances and Trends. *Biosensors (Basel)* **2017**, *7* (4), 62.
(2) Wang, C.; Liu, M.; Wang, Z.; Li, S.; Deng, Y.; He, N. Point-of-Care Diagnostics for Infectious Diseases: From Methods to Devices. *Nano Today* **2021**, *37*, 101092.
(3) Xue, T.; Liang, W.; Li, Y.; Sun, Y.; Xiang, Y.; Zhang, Y.; Dai, Z.; Duo, Y.; Wu, L.; Qi, K.; Shivananju, B. N.; Zhang, L.; Cui, X.; Zhang, H.; Bao, Q. Ultrasensitive Detection of MiRNA with an Antimonene-Based Surface Plasmon Resonance Sensor. *Nat. Commun.* **2019**, *10* (1), 1−9.
(4) Alafeef, M.; Dighe, K.; Moitra, P.; Pan, D. Rapid, Ultrasensitive, and Quantitative Detection of SARS-CoV-2 Using Antisense Oligonucleotides Directed Electrochemical Biosensor Chip. *ACS Nano* **2020**, *14* (12), 17028−17045.
(5) Hwang, M. T.; Heiranian, M.; Kim, Y.; You, S.; Leem, J.; Taqieddin, A.; Faramarzi, V.; Jing, Y.; Park, I.; van der Zande, A. M.; Nam, S.; Aluru, N. R.; Bashir, R. Ultrasensitive Detection of Nucleic Acids Using Deformed Graphene Channel Field Effect Biosensors. *Nat. Commun.* **2020**, *11* (1), 1−11.
(6) Samani, S. S.; Khojastehnezhad, A.; Ramezani, M.; Alibolandi, M.; Yazdi, F. T.; Mortazavi, S. A.; Khoshbin, Z.; Abnous, K.; Taghdisi, S. M. Ultrasensitive Detection of Micrococcal Nuclease Activity and Staphylococcus Aureus Contamination Using Optical Biosensor Technology-A Review. *Talanta* **2021**, *226*, 122168.
(7) Moreda-Pineiro, A.; Sanchez-Gonzalez, J.; Chantada-Vazquez, M. P.; Bermejo, A. M.; Bermejo-Barrera, P. MIPs as a Versatile Tool for Micro-Solid-Phase Extraction and Probe Sensing. *Curr. Chem. Biol.* **2018**, *12* (2), 114−134.
(8) Mpupa, A.; Selahle, S. K.; Mizaikoff, B.; Nomngongo, P. N. Recent Advances in Solid-Phase Extraction (SPE) Based on Molecularly Imprinted Polymers (MIPs) for Analysis of Hormones. *Chemosensors* **2021**, *9* (7), 151.
(9) Guo, X.; Li, J.; Arabi, M.; Wang, X.; Wang, Y.; Chen, L. Molecular-Imprinting-Based Surface-Enhanced Raman Scattering Sensors. *ACS Sens.* **2020**, *5* (3), 601−619.
(10) Tarannum, N.; Hendrickson, O. D.; Khatoon, S.; Zherdev, A. v.; Dzantiev, B. B. Molecularly Imprinted Polymers as Receptors for Assays of Antibiotics. *Critical Reviews in Environmental Science and Technology* **2020**, *50* (4), 291−310.
(11) Lowdon, J. W.; Diliën, H.; Singla, P.; Peeters, M.; Cleij, T. J.; van Grinsven, B.; Eersels, K. MIPs for Commercial Application in Low-Cost Sensors and Assays − An Overview of the Current Status Quo. *Sens Actuators B Chem.* **2020**, *325*, 128973.
(12) Wang, P.; Zhu, H.; Liu, J.; Ma, Y.; Yao, J.; Dai, X.; Pan, J. Double Affinity Integrated MIPs Nanoparticles for Specific Separation of Glycoproteins: A Combination of Synergistic Multiple Bindings and Imprinting Effect. *Chem. Eng. J.* **2019**, *358*, 143−152.
(13) Shevchenko, K. G.; Garkushina, I. S.; Canfarotta, F.; Piletsky, S. A.; Barlev, N. A. Nano-Molecularly Imprinted Polymers (NanoMIPs) as a Novel Approach to Targeted Drug Delivery in Nanomedicine. *RSC Adv.* **2022**, *12* (7), 3957−3968.
(14) Zaidi, S. A. Molecular Imprinting: A Useful Approach for Drug Delivery. *Mater. Sci. Energy Technol.* **2020**, *3*, 72−77.
(15) Zaidi, S. A. Molecular Imprinting Polymers and Their Composites: A Promising Material for Diverse Applications. *Biomater Sci.* **2017**, *5* (3), 388−402.
(16) Singh, M.; Singh, S.; Singh, S. P.; Patel, S. S. Recent Advancement of Carbon Nanomaterials Engrained Molecular Imprinted Polymer for Environmental Matrix. *Trends in Environmental Analytical Chemistry* **2020**, *27*, No. e00092.
(17) Teixeira, S. P. B.; Reis, R. L.; Peppas, N. A.; Gomes, M. E.; Domingues, R. M. A. Epitope-Imprinted Polymers: Design Principles of Synthetic Binding Partners for Natural Biomacromolecules. *Sci. Adv.* **2021**, *7* (44), 9884−9913.
(18) Ye, L. Synthetic Strategies in Molecular Imprinting. *Molecularly Imprinted Polymers in Biotechnology*; Springer International Publishing, 2015; Vol. *150*, pp 1−24.
(19) Svenson, J.; Nicholls, I. A. On the Thermal and Chemical Stability of Molecularly Imprinted Polymers. *Anal. Chim. Acta* **2001**, *435* (1), 19−24.
(20) Cheong, W. J.; Ali, F.; Choi, J. H.; Lee, J. O.; Yune Sung, K. Recent Applications of Molecular Imprinted Polymers for Enantio-Selective Recognition. *Talanta* **2013**, *106*, 45−59.
(21) Ramanavicius, S.; Jagminas, A.; Ramanavicius, A. Advances in Molecularly Imprinted Polymers Based Affinity Sensors (Review). *Polymers* **2021**, *13* (6), 974.
(22) Rebelo, P.; Costa-Rama, E.; Seguro, I.; Pacheco, J. G.; Nouws, H. P. A.; Cordeiro, M. N. D. S.; Delerue-Matos, C. Molecularly Imprinted Polymer-Based Electrochemical Sensors for Environmental Analysis. *Biosens Bioelectron* **2021**, *172*, 112719.
(23) Rebelo, R.; Barbosa, A. I.; Correlo, V. M.; Reis, R. L. An Outlook on Implantable Biosensors for Personalized Medicine. *Engineering* **2021**, *7* (12), 1696−1699.
(24) Chu, T.-X.; Vu, V.-P.; Tran, H.-T.; Tran, T.-L.; Tran, Q.-T.; Le Manh, T. Molecularly Imprinted Polyaniline Nanowire-Based Electrochemical Biosensor for Chloramphenicol Detection: A Kinetic Study of Aniline Electropolymerization. *J. Electrochem. Soc.* **2020**, *167* (2), 027527.
(25) Zaidi, S. A. Molecular Imprinting: A Useful Approach for Drug Delivery. *Mater. Sci. Energy Technol.* **2020**, *3*, 72−77.
(26) Xu, S.; Wang, L.; Liu, Z. Molecularly Imprinted Polymer Nanoparticles: An Emerging Versatile Platform for Cancer Therapy. *Angew. Chem., Int. Ed.* **2021**, *60* (8), 3858−3869.
(27) Cunliffe, D.; Kirby, A.; Alexander, C. Molecularly Imprinted Drug Delivery Systems. *Adv. Drug Deliv Rev.* **2005**, *57* (12), 1836−1853.
(28) Xiao, D.; Jiang, Y.; Bi, Y. Molecularly Imprinted Polymers for the Detection of Illegal Drugs and Additives: A Review. *Microchimica Acta* **2018**, *185* (4), 1−20.
(29) Zhang, H. Molecularly Imprinted Nanoparticles for Biomedical Applications. *Adv. Mater.* **2020**, *32* (3), 1806328.
(30) Ansell, R. J. Characterization of the Binding Properties of Molecularly Imprinted Polymers. In *Molecularly Imprinted Polymers in Biotechnology*; Mattiasson, B., Ye, L., Eds.; Springer: Heidelberg, 2015; Vol. *150*, pp 51−93.
(31) Corton, E.; García-Calzón, J. A.; Díaz-García, M. E. Kinetics and Binding Properties of Cloramphenicol Imprinted Polymers. *J. Non Cryst. Solids* **2007**, *353* (8−10), 974−980.
(32) Nightingale, A. M.; Leong, C. L.; Burnish, R. A.; Hassan, S. ul; Zhang, Y.; Clough, G. F.; Boutelle, M. G.; Voegeli, D.; Niu, X. Monitoring Biomolecule Concentrations in Tissue Using a Wearable Droplet Microfluidic-Based Sensor. *Nature Communications 2019 10:1* **2019**, *10* (1), 1−12.
(33) Zhang, J.; Zhang, M.; Tang, K.; Verpoort, F.; Sun, T. Polymer-Based Stimuli-Responsive Recyclable Catalytic Systems for Organic Synthesis. *Small* **2014**, *10* (1), 32−46.
(34) Tan, S.; Saito, K.; Hearn, M. T. Stimuli-Responsive Polymeric Materials for Separation of Biomolecules. *Curr. Opin Biotechnol* **2018**, *53*, 209−223.
(35) Zhang, J.; Hao, Y.; Tian, X.; Liang, Y.; He, X.; Gao, R.; Chen, L.; Zhang, Y. Multi-Stimuli Responsive Molecularly Imprinted Nanoparticles with Tailorable Affinity for Modulated Specific Recognition of Human Serum Albumin. *J. Mater. Chem. B* **2022**, *10* (35), 6634.
(36) González, G. P.; Hernando, P. F.; Alegría, J. S. D. A Morphological Study of Molecularly Imprinted Polymers Using the Scanning Electron Microscope. *Anal. Chim. Acta* **2006**, *557* (1−2), 179−183.

https://doi.org/10.1021/acsnano.2c11618
ACS Nano 2023, 17, 5632−5643

(37) Weber, A.; Dettling, M.; Brunner, H. Isothermal titration calorimetry of molecularly imprinted polymer nanospheres. *Macromol. Rapid Commun.* **2002**, *23* (14), 824−828.
(38) Weickenmeier, M.; Wenz, G. Cyclodextrin Sidechain Polyesters — Synthesis and Inclusion of Adamantan Derivatives. *Macromol. Rapid Commun.* **1996**, *17* (10), 731−736.
(39) Kirchner, R.; Seidel, J.; Wolf, G.; Wulff, G. Calorimetric Investigation of Chiral Recognition Processes in a Molecularly Imprinted Polymer. *J. Incl Phenom Macrocycl Chem.* **2002**, *43*, 279−283.
(40) Cui, X. T.; Zhou, D. D. Poly (3,4-Ethylenedioxythiophene) for Chronic Neural Stimulation. *IEEE Transactions on Neural Systems and Rehabilitation Engineering* **2007**, *15* (4), 502−508.
(41) Koutsouras, D. A.; Gkoupidenis, P.; Stolz, C.; Subramanian, V.; Malliaras, G. G.; Martin, D. C. Impedance Spectroscopy of Spin-Cast and Electrochemically Deposited PEDOT:PSS Films on Microfabricated Electrodes with Various Areas. *ChemElectroChem.* **2017**, *4* (9), 2321−2327.
(42) Bianchi, M.; Carli, S.; di Lauro, M.; Prato, M.; Murgia, M.; Fadiga, L.; Biscarini, F. Scaling of Capacitance of PEDOT:PSS: Volume vs. Area. *J. Mater. Chem. C Mater.* **2020**, *8* (32), 11252−11262.
(43) Yang, M.; Zhang, Y.; Zhang, H.; Li, Z. Characterization of PEDOT:PSS as a Biocompatible Conductive Material. *2015 IEEE 10th International Conference on Nano/Micro Engineered and Molecular Systems*, Xi'an, China, April 7−11, 2015; pp 149−151.
(44) Liu, X.; Liu, J. Biosensors and Sensors for Dopamine Detection. *View* **2021**, *2* (1), 20200102.
(45) Rivera-Serrano, N.; Pagan, M.; Colón-Rodríguez, J.; Fuster, C.; Vélez, R.; Almodovar-Faria, J.; Jiménez-Rivera, C.; Cunci, L. Static and Dynamic Measurement of Dopamine Adsorption in Carbon Fiber Microelectrodes Using Electrochemical Impedance Spectroscopy. *Anal. Chem.* **2018**, *90* (3), 2293.
(46) Qian, T.; Yu, C.; Zhou, X.; Ma, P.; Wu, S.; Xu, L.; Shen, J. Ultrasensitive Dopamine Sensor Based on Novel Molecularly Imprinted Polypyrrole Coated Carbon Nanotubes. *Biosens. Bioelectron.* **2014**, *58*, 237−241.
(47) Kaya, H. K.; Cinar, S.; Altundal, G.; Bayramlı, Y.; Unaleroglu, C.; Kuralay, F. A Novel Design Thia-Bilane Structure-Based Molecular Imprinted Electrochemical Sensor for Sensitive and Selective Dopamine Determination. *Sens Actuators B Chem.* **2021**, *346*, 130425.
(48) Zhang, W.; Duan, D.; Liu, S.; Zhang, Y.; Leng, L.; Li, X.; Chen, N.; Zhang, Y. Metal-Organic Framework-Based Molecularly Imprinted Polymer as a High Sensitive and Selective Hybrid for the Determination of Dopamine in Injections and Human Serum Samples. *Biosens Bioelectron* **2018**, *118*, 129−136.
(49) Khadem-Abbassi, K.; Rinnert, H.; Balan, L.; Doumandji, Z.; Joubert, O.; Masteri-Farahani, M.; Schneider, R. $CdTe_{0.5}S_{0.5}$/ZnS Quantum Dots Embedded in a Molecularly Imprinted Polymer for the Selective Optosensing of Dopamine. *Nanomaterials* **2019**, *9* (5), 693.
(50) Yang, J.; Hu, Y.; Li, Y. Molecularly Imprinted Polymer-Decorated Signal on-off Ratiometric Electrochemical Sensor for Selective and Robust Dopamine Detection. *Biosens Bioelectron* **2019**, *135*, 224−230.
(51) Li, N.; Nan, C.; Mei, X.; Sun, Y.; Feng, H.; Li, Y. Electrochemical Sensor Based on Dual-Template Molecularly Imprinted Polymer and Nanoporous Gold Leaf Modified Electrode for Simultaneous Determination of Dopamine and Uric Acid. *Microchimica Acta* **2020**, *187* (9), 1−10.
(52) Kamel, A. H.; Amr, A. E. G. E.; Ashmawy, N. H.; Galal, H. R.; Al-Omar, M. A.; Sayed, A. Y. A. Solid-Contact Potentiometric Sensors Based on Stimulus-Responsive Imprinted Polymers for Reversible Detection of Neutral Dopamine. *Polymers* **2020**, *12* (6), 1406.
(53) Kaya, H. K.; Cinar, S.; Altundal, G.; Bayramlı, Y.; Unaleroglu, C.; Kuralay, F. A Novel Design Thia-Bilane Structure-Based Molecular Imprinted Electrochemical Sensor for Sensitive and Selective Dopamine Determination. *Sens Actuators B Chem.* **2021**, *346*, 130425.
(54) Tang, K.; Turner, C.; Case, L.; Mehrehjedy, A.; He, X.; Miao, W.; Guo, S. Organic Electrochemical Transistor with Molecularly Imprinted Polymer-Modified Gate for the Real-Time Selective Detection of Dopamine. *ACS Appl. Polym. Mater.* **2022**, *4* (4), 2337−2345.
(55) Jimenez, M.; Garcia-Carmona, F.; Garcia-Canovas, F.; Iborra, J. L.; Lozano, J. A.; Martinez, F. Chemical Intermediates in Dopamine Oxidation by Tyrosinase, and Kinetic Studies of the Process. *Arch. Biochem. Biophys.* **1984**, *235* (2), 438−448.
(56) Kopke, D. L.; Broadie, K. FM Dye Cycling at the Synapse: Comparing High Potassium Depolarization, Electrical and Channelrhodopsin Stimulation. *J. Vis Exp* **2018**, *2018* (135), 57765.
(57) Takashima, A.; Koike, T. Relationship between Dopamine Content and Its Secretion in PC12 Cells as a Function of Cell Growth. *BBA - Molecular Cell Research* **1985**, *847* (1), 101−107.
(58) Westerink, R. H. S.; Ewing, A. G. The PC12 Cell as Model for Neurosecretion. *Acta Physiol (Oxf)* **2008**, *192* (2), 273.
(59) Suedee, R.; Seechamnanturakit, V.; Suksuwan, A.; Canyuk, B. Recognition Properties and Competitive Assays of a Dual Dopamine/Serotonin Selective Molecularly Imprinted Polymer. *Int. J. Mol. Sci.* **2008**, *9* (12), 2333−2356.
(60) Duff, M. R.; Grubbs, J.; Howell, E. E. Isothermal Titration Calorimetry for Measuring Macromolecule-Ligand Affinity. *J. Vis Exp* **2011**, *55* (55), 2796.
(61) Benoudjit, A.; Bader, M. M.; Wan Salim, W. W. A. Study of Electropolymerized PEDOT:PSS Transducers for Application as Electrochemical Sensors in Aqueous Media. *Sens Biosensing Res.* **2018**, *17*, 18−24.
(62) Cui, X.; Martin, D. C. Electrochemical Deposition and Characterization of Poly(3,4-Ethylenedioxythiophene) on Neural Microelectrode Arrays. *Sens Actuators B Chem.* **2003**, *89* (1−2), 92−102.
(63) Krukiewicz, K.; Kowalik, A.; Czerwinska-Glowka, D.; Biggs, M. J. P. Electrodeposited Poly(3,4-Ethylenedioxypyrrole) Films as Neural Interfaces: Cytocompatibility and Electrochemical Studies. *Electrochim. Acta* **2019**, *302*, 21−30.
(64) Parlak, O.; Keene, S. T.; Marais, A.; Curto, V. F.; Salleo, A. Molecularly Selective Nanoporous Membrane-Based Wearable Organic Electrochemical Device for Noninvasive Cortisol Sensing. *Sci. Adv.* **2018**, *4* (7), eaar2904.
(65) Cui, M. R.; Zhao, W.; Li, X. L.; Xu, C. H.; Xu, J. J.; Chen, H. Y. Simultaneous Monitoring of Action Potentials and Neurotransmitter Release from Neuron-like PC12 Cells. *Anal. Chim. Acta* **2020**, *1105*, 74−81.
(66) Lah, J. J.; Burry, R. W. Neuronotypic Differentiation Results in Reduced Levels and Altered Distribution of Synaptophysin in PC 12 Cells. *J. Neurochem* **1993**, *60* (2), 503−512.

https://doi.org/10.1021/acsnano.2c11618
ACS Nano 2023, 17, 5632−5643